

HST Imaging of $z > 0.4$ Quasar Host Galaxies Selected by Quasar Radio and Optical Properties¹

Eric J. Hooper², Chris D. Impey², and Craig B. Foltz³

ABSTRACT

A sample of 16 quasars selected from the Large Bright Quasar Survey in the redshift range $0.4 < z < 0.5$ has been imaged in the R band with the Planetary Camera on the WFPC2 instrument of the Hubble Space Telescope. The host galaxy magnitudes are mostly similar to or brighter than L^* , and the host luminosity is positively correlated with the luminosity of the quasar nuclear component. There is no distinction in host galaxy magnitude between radio-loud and radio-quiet quasars, assuming they are all of the same galaxy type. Many of the host galaxies in the sample have small axial ratios, which may indicate that they are inclined disk systems. Alternatively, this elongated appearance may be due to bars or other distinctive morphological features which are visible while the bulk of the underlying lower surface brightness components of the host galaxy are not.

Subject headings: galaxies:active – quasars:general

¹ Accepted for publication in the Astrophysical Journal Letters. This work is based on observations with the NASA/ESA Hubble Space Telescope, obtained at the Space Telescope Science Institute, which is operated by the Association of Universities for Research in Astronomy, Inc., under NASA contract NAS 5-26555

²Steward Observatory, The University of Arizona, Tucson, AZ 85721
ehooper@as.arizona.edu, cimpey@as.arizona.edu

³Multiple Mirror Telescope Observatory, The University of Arizona, Tucson, AZ 85721
cfoltz@as.arizona.edu

1. Introduction

The refurbished Hubble Space Telescope (HST) has provided a substantial boost to the study of quasar host galaxies because of its ability to resolve the inner structures of the hosts close to the quasar nucleus. Most quasars imaged to date with HST lie at redshifts $z < 0.3$ and have low to moderate nuclear source luminosities (Bahcall, Kirhakos, & Schneider 1994, 1995a, 1996; Hutchings et al. 1994; Boyce et al. 1997), although Bahcall, Kirhakos, & Schneider (1995b) and Disney et al. (1995) include objects with $M_V \approx -27$ in the cosmology adopted for this paper ($H_0 = 50 \text{ km s}^{-1} \text{ Mpc}^{-1}$, $q_0 = 0.5$). The detected host galaxies are typically at least as bright as the Schechter function’s characteristic luminosity L^* , but several undetected hosts have estimated upper limits of $\leq L^*$ (Bahcall et al. 1995b). The most recent determination of L^* in the R passband is $M_R^* = -21.8$ (Lin et al. 1996). While classifying the host galaxies as either disk or elliptical systems is often difficult because of contamination by the quasar and the frequent occurrence of disturbed morphologies, most hosts detected to date in the HST observations appear to have luminosity distributions consistent with early-type galaxies (Disney et al. 1995; Bahcall et al. 1997; and summarized in McLeod & Rieke 1995b). Radio-quiet quasars, which were once thought to reside in spiral host galaxies (e.g., Smith et al. 1986), appear to exist in both elliptical (e.g., Hutchings & Morris 1995) and disk (e.g., Hutchings et al. 1994) systems. Several of the hosts appear to be involved in interactions or mergers (e.g., Bahcall, Kirhakos, & Schneider 1995a), especially the hosts of infrared luminous quasars (Hutchings & Morris 1995; Boyce et al. 1997).

2. The Sample

Candidates for this study were selected from the Large Bright Quasar Survey (LBQS; Hewett, Foltz, & Chaffee 1995 and references therein), the largest homogeneous optical quasar survey to date, containing over 1000 quasars in the redshift range $0.2 < z < 3.4$. The LBQS was compiled from digitized UK Schmidt objective prism plates, with candidates selected based on one or more well-defined selection criteria: (1) blue color; (2) strong emission or absorption features; or (3) strong continuum breaks. Advantages of the survey include: (1) $> 99\%$ success rate in classifying candidates; (2) sensitivity to almost all known types of quasars, with the exceptions of the rare classes of objects with red featureless continua or large-amplitude photometric variations; (3) detection efficiency that varies smoothly and monotonically with redshift; (4) quantifiable selection criteria, enabling the calculation of the selection probability as a function of quasar luminosity, redshift, and spectral energy distribution; and (5) the inclusion of candidates whose images on the

discovery plates are resolved due to an underlying host galaxy.

This last point is particularly important for studies such as this one. Several previous optically selected quasar surveys required that a candidate appear point-like, a seeing-dependent and often subjective criterion which could potentially exclude quasars with bright host galaxies. Quasars with typical colors and emission line strengths at the redshifts of the sample selected for WFPC2 imaging satisfy the LBQS magnitude limit and selection criteria as long as the total luminosity of the host galaxy is approximately equal to or less than that of the quasar (Hooper et al. 1995; Hewett et al. 1995). Since the absolute magnitudes of the quasars in the HST sample fall in the range $-25 < M_B < -23$, very few known galaxies would be excluded *a priori*.

The radio properties of the LBQS have been studied using pointed Very Large Array 8.4 GHz snapshots of 1/3 of the sample (359 targets), reaching a median detection threshold of about 0.3 mJy (Hooper et al. 1996). The fraction of radio-loud quasars (8.4 GHz luminosity $> 10^{25}$ W Hz $^{-1}$) is constant at $\approx 10\%$ within the errors over almost the full redshift range of the survey and across nearly the entire absolute magnitude range ($-28 < M_B < -23$). The only changes occur at the brightest absolute magnitudes, $M_B < -28$, where the radio-loud fraction rises to $\approx 30\%$, and there is also a slight rise around $z \approx 1$.

Selection of targets for WFPC2 imaging was dictated by several desiderata: (1) a radio luminosity span typical of optically selected quasars; (2) nearly identical redshifts to avoid problems of interpretation due to evolution and to provide a uniform rest-frame spatial resolution scale; and (3) quasar absolute magnitudes bright enough to exclude Seyfert galaxies, yet not so bright that the nucleus completely obscures the host galaxy. LBQS quasars in the redshift range $0.4 < z < 0.5$ satisfy these criteria. All six known LBQS radio-loud quasars within this redshift interval were selected. These objects have radio luminosities ranging up to 3×10^{26} W Hz $^{-1}$. Ten quasars with 8.4 GHz luminosities $\leq 10^{23.5}$ W Hz $^{-1}$, well below the radio-loud threshold, were selected to complete the sample. The radio-quiet quasars were chosen semi-uniformly from the absolute magnitude range $-25 < M_B < -23$, an interval containing nearly all of the LBQS quasars with redshifts $0.4 < z < 0.5$.

3. Data Reduction and Analysis

The quasars were centered on the Planetary Camera (0.046 arcseconds per pixel) of WFPC2 and imaged through the F675W filter, which approximates Johnson *R*. Total integration times of 20 to 30 minutes were divided into 3 or 4 separate exposures to avoid

saturation of the quasar core and to facilitate cosmic-ray removal. The gain was set to 14 electrons per DN in all exposures. Readnoise, 7 electrons on the PC, and digitization effects dominated photon noise from the background in all of the images. The pipeline data reduction products were used, which are corrected for bias, dark current, and flat-fielding.

The reduced data were analyzed by cross-correlating two-dimensional (2-D) galaxy and point spread function (psf) models with the data to determine the optimal values of host galaxy flux, exponential scalelength or effective radius, axial ratio, and position angle, as well as the quasar centroid and flux. A description of the general 2-D cross-correlation method was presented by Phillipps & Davies (1991); Boyce, Phillipps, & Davies (1993) discussed its application specifically to quasar host galaxy analysis. Advantages of this method include higher accuracy and sensitivity than one-dimensional profile fitting, accurate determination of the flux of the quasar nucleus even in low S/N data where the nature of the host galaxy is rather uncertain, and relative insensitivity to missing data or the presence of other nearby galaxies. Two-dimensional models consisting of a psf, generated with the “Tiny Tim” software (Krist 1996), and either a disk or elliptical galaxy component were repeatedly cross-correlated with the region around the quasar in the WFPC2 images while varying the psf and model galaxy parameters. The set of parameters which maximized the cross-correlation function was adopted. The 2-D technique was checked by analyzing one-dimensional (1-D) profiles derived from elliptical isophote fits to the more prominent host galaxies, cases in which this older method is still expected to be fairly robust. The magnitudes from the 1-D technique were typically ≈ 0.3 mag brighter than those from the cross-correlation.

Fluxes were converted to Johnson R using Equation (8) in Holtzman et al. (1995). This conversion has a color term of < 0.15 mag for typical disk and elliptical galaxy and quasar colors at $z \approx 0.5$. Colors for galaxies and quasars, as well as k -corrections for conversion to rest-frame absolute magnitudes, were obtained from Coleman, Wu, & Weedman (1980) and Cristiani & Vio (1990), respectively. Minor (≤ 0.1 mag) corrections were applied to the derived magnitudes to account for charge transfer efficiency effects and for differences in the flux measurement methods between the calibration of the WFPC2 photometric system and the LBQS data, as described in Holtzman et al. (1995).

4. Results

Numerical results of the analysis are presented in Table 1, which lists for each target: (1) source name; (2) redshift from Hewett et al. (1995); (3) 8.4 GHz luminosity (W Hz^{-1}) from Hooper et al. (1995, 1996); (4) and (5) apparent and absolute R magnitudes for the

quasar nuclear component, respectively; apparent (6) and (7) absolute R magnitudes for the host galaxy using an exponential disk template; (8) and (9) apparent and absolute R magnitudes for an $r^{1/4}$ model template; and (10) the axial ratio of the host galaxy. The quasar magnitudes are relatively insensitive to the galaxy template used in the analysis, differing by typically 2% or less between the two models; the average of the derived quasar magnitudes is listed in columns (4) and (5). The integrated host galaxy fluxes, however, are typically 0.5 to 1 magnitude fainter for the disk model, and both are listed in the table. Axial ratios derived from the two models are identical in most cases, and the average is listed in the few that are not.

Scaled 2-D psfs, normalized to the flux derived for the nuclear point source, were subtracted from the images in order to better see the host galaxies. The region around each quasar is shown in Fig. 1 before (left column) and after (right column) psf subtraction. The stretch was adjusted to show the faint outer isophotes in most cases, although the hard-copy reproduction quality of these faint features is poor. Each pixel corresponds to a projected distance of 310 pc at $z = 0.45$, the midpoint of the redshift range of the sample, $0.4 < z < 0.5$. The psf subtracted images contain a discontinuity at the center where the quasar component has been subtracted. This is an artifact of the subtraction and is found after a scaled psf is subtracted from a stellar image. The discontinuity often appears as a small negative feature in the images unless the central surface brightness of the host galaxy is relatively high. Apparent companion objects lying very close to the quasar were included in the displayed field. Many of the fields contain extended objects on the PC images which are not shown here. The two point-like features close to the quasar 0100+0205 are likely to be artifacts associated with the diffraction spikes.

Rigorous analysis of the uncertainties in the derived parameters and determination of the limiting magnitude of a detectable host galaxy are challenging problems, which will be addressed in a subsequent paper. However, some information on the reliability of the analysis technique and detection sensitivity was obtained by applying the 2-D cross-correlation method to stars found in the Planetary Camera quasar fields. Comparison with the quasar results is complicated by the fact that the stars are typically substantially fainter than the quasars. The brightest star analyzed, in the field of 1218+1734, had $R = 20.02$, 0.5 mag fainter than the faintest quasars in the sample (0020+0018 and 1209+1259). The “host galaxy” magnitudes produced for this star were $R = 21.71$ and $R = 22.23$ for the elliptical and disk templates, respectively, in each case at least 1.4 mag fainter than the results for the quasars. One quasar, 1243+1701, had a very low axial ratio of 0.1 and an unphysically small effective radius and exponential scalelength of ≤ 300 pc. Either there is little or no detectable flux from the host galaxy, or the host has an unusual morphology and low surface brightness, for which the standard templates are inadequate.

Some extended residual emission is seen in the psf subtracted image of this field (Fig. 1). The small companion very close to the quasar did not affect the analysis, since similar results were obtained after it had been removed from the image. Until additional analysis is performed, it is not certain whether a host has been detected for this quasar or others which have faint extended emission only in the near vicinity of the quasar nucleus. Consequently, the discussion that follows will consider both the entire sample and a subset consisting of the most clearly visible host galaxies.

5. Discussion

Absolute R magnitude (M_R) of the quasar nuclear component is plotted against host galaxy M_R derived from $r^{1/4}$ and disk templates in Fig. 2, with radio-loud and radio-quiet quasars denoted by filled circles and stars respectively. The detected host galaxies are luminous; magnitudes derived from $r^{1/4}$ fits and from many of the disk fits are brighter than $M_R^* = -21.8$ (Lin et al. 1996). Published values of L^* differ by up to 1 mag, but this does not alter the basic result that the elliptical fits are mostly brighter than the characteristic luminosity, while the magnitude distribution derived from disk templates straddles L^* . Note in particular that there is not a dominant population of low-luminosity host galaxies in the LBQS sample. Host galaxy luminosity is positively correlated with quasar nuclear luminosity at the 99% confidence level for the $r^{1/4}$ and disk template magnitudes, as indicated by a Kendall's τ test. This correlation is consistent with the existence of a minimum host galaxy luminosity which increases with quasar luminosity, a trend noted by McLeod & Rieke (1995a,b) using H -band host galaxy magnitudes in lower-redshift samples. The lower bound to the host galaxy luminosities, converted to R -band, is about 0.5 (disk template) or 1.5 (elliptical template) mag fainter than the lower luminosity envelope of the LBQS host galaxies. The host galaxy magnitudes deviate from this trend, becoming roughly constant with quasar magnitude, for quasars fainter than $M_R \approx -24$. A similar break occurs at roughly the same magnitude, after adjusting for differences in passband and cosmology, in the McLeod & Rieke (1995a,b) data. The radio-loud quasars all lie in the brighter half of the range of quasar nuclear M_R . This was not an effect of the selection of the radio-loud quasars, as the majority were in the fainter half of the range of M_B . There is no apparent distinction between the host galaxy magnitudes of radio-loud and radio-quiet quasars with similar nuclear component luminosities for a single type of galaxy template. However, if the host galaxy morphologies differ between radio luminosity classes, such that radio-loud quasars are in ellipticals and radio-quiet nuclei reside in spirals, then the hosts of luminous radio sources would be consistently brighter by about one magnitude.

The axial ratios derived for the host galaxies have a median of 0.5, with only two objects having ratios > 0.6 . These values are significantly lower than is typical for elliptical galaxies, which generally appear less elongated. A Kolmogorov-Smirnov (KS) test indicates that the distribution of axial ratios in a sample of 171 elliptical galaxies from Ryden (1992) differs from the LBQS results at a confidence level $> 99.99\%$. Fewer than 5% of the ellipticals have axial ratios < 0.6 , where the bulk of the LBQS objects lie. This result may indicate that the LBQS sample consists primarily of inclined disk systems, which differs from the conclusion of several other HST imaging studies that early type host galaxies are prevalent, even among radio-quiet objects. McLeod & Rieke (1994a,b) did not find any host galaxies with measurable axial ratios < 0.5 in a sample drawn from the PG quasar survey, even among galaxies which appeared to be spirals. They attributed the lack of inclined disk systems to the additional reddening of the active nucleus caused by this viewing geometry, which would cause the quasar to fail the UV-excess selection criterion of the PG. Increased extinction would also remove potential candidates by making them fainter than the PG magnitude limit. However, very few quasars which are intrinsically too bright to be included in the PG would cross the magnitude selection boundary of the survey due to extinction from an inclined host, because the bright flux limit of the PG exceeds the apparent fluxes of virtually all known quasars. The LBQS selection is based on spectral features in addition to color, and its bright magnitude limit is roughly coincident with the faint limit of the PG, so it is reasonable to expect that spiral host galaxies with higher inclinations could be included in the LBQS. Another possibility is that the detected portions of some of the host galaxies are bars, particularly in the cases of very low axial ratios. These systems could have nearly face-on disks which are too faint to detect, leaving only the bar components visible.

Half of the sample, the 8 targets with the most obvious host galaxies in Fig. 1, was examined separately to ensure that the major results are not skewed by the lower surface brightness host galaxies, for which only marginal emission is seen and which may not have been detected in some cases. This subsample contains 3 radio-loud quasars (1222+1235, 1230–0015, and 2348+0210) and 5 radio-quiet (0020+0018, 0021–0301, 1149+0043, 1222+1010, 2214–1903). The absolute magnitudes of the quasar nuclear components in these objects span the range of the full sample. A correlation with host galaxy luminosity is still suggested visually, particularly among the more luminous quasars, but the trend is too weak given the reduced sample size to produce a significant result from the Kendall's τ test (86% confidence). Radio-loud and radio-quiet quasars with similar central component magnitudes in the subsample have similar host galaxy luminosities when derived from the same class of galaxy template. Only one host galaxy in the restricted sample has an axial ratio > 0.6 , and the flattened morphologies of the remaining objects can be easily seen in most cases in Fig. 1. The KS test using Ryden's (1992) sample of elliptical galaxies

was repeated, with the conservative assumption that the host galaxies not included in the subsample had relatively round morphologies closely matching the axial ratio distribution of the ellipticals. The two distributions were different at $> 99\%$ confidence level, indicating that there is a significant component of clearly flattened systems in the LBQS sample.

The authors thank Alice Quillen, Gary Schmidt, and Joe Pesce for helpful discussions and the referee, Donald Schneider, for constructive input. This work was supported by NASA through GO program grant number 5450 from the Space Telescope Science Institute, which is operated by the Association of Universities for Research in Astronomy, Inc., under NASA contract NAS 5-26555. Additional support was provided by a NASA Graduate Student Researchers Program Fellowship (EJH), grant number NGT-51152. This research has made use of the NASA Astrophysics Data System (ADS).

REFERENCES

- Bahcall, J. N., Kirhakos, S., Saxe, D. H., & Schneider, D. P. 1997, *ApJ*, in press
- Bahcall, J. N., Kirhakos, S., & Schneider, D. P. 1994, *ApJ*, 435, L11
- Bahcall, J. N., Kirhakos, S., & Schneider, D. P. 1995a, *ApJ*, 447, L1
- Bahcall, J. N., Kirhakos, S., & Schneider, D. P. 1995b, *ApJ*, 450, 486
- Bahcall, J. N., Kirhakos, S., & Schneider, D. P. 1996, *ApJ*, 457, 557
- Boyce, P. J., Phillipps, S., & Davies, J. I. 1993, *A&A*, 280, 694
- Boyce, P. J., et al. 1997, *ApJ*, in press
- Coleman, G. D., Wu, C., & Weedman, D. W. 1980, *ApJS*, 43, 393
- Cristiani, S., & Vio, R. 1990, *A&A*, 227, 385
- Disney et al. 1995, *Nature*, 376, 150
- Hewett, P. C., Foltz, C. B., & Chaffee, F. H. 1995, *AJ*, 109, 1498
- Holtzman, J. A., Burrows, C. J., Casertano, S., Hester, J. J., Trauger, J. T., Watson, A. M., & Worthey, G. 1995, *PASP*, 107, 1065
- Hooper, E. J., Impey, C. D., Foltz, C. B., & Hewett, P. C. 1995, *ApJ*, 445, 62
- Hooper, E. J., Impey, C. D., Foltz, C. B., & Hewett, P. C. 1996, *ApJ*, 473, 746
- Hutchings, J. B., Holtzman, J., Sparks, W. B., Morris, S. C., Hanisch, R. J., & Mo, J. 1994, *ApJ*, 429, L1
- Hutchings, J. B., & Morris, S. C. 1995, *AJ*, 109, 1541
- Krist, J. 1996, *The Tiny Tim User's Manual*, version 4.1
- Lin, H., Kirshner, R. P., Schectman, S. A., Landy, S. D., Oemler, A., Tucker, D. L., & Schechter, P. L. 1996, *ApJ*, 464, 60
- McLeod, K. K., & Rieke, G. H. 1994a, *ApJ*, 420, 58
- McLeod, K. K., & Rieke, G. H. 1994b, *ApJ*, 431, 137
- McLeod, K. K., & Rieke, G. H. 1995a, *ApJ*, 441, 96
- McLeod, K. K., & Rieke, G. H. 1995b, *ApJ*, 454, L77
- Phillipps, S., & Davies, J. 1991, *MNRAS*, 251, 105
- Ryden, B. S. 1992, *ApJ*, 396, 445

Smith, E. P., Heckman, T. M., Bothun, G. D., Romanishin, W., & Balick, B. 1986, *ApJ*,
306, 64

6. Figure Captions

Fig. 1.— Each pair of linearly stretched grayscale images across the page shows the field around one of the quasars in the sample. The quasar and its host galaxy are shown in the left panel, and the same field after the nuclear component has been subtracted is displayed in the right panel. A direction indicator (the arrow points north and the other line east) and size scale are printed between each pair of panels. The LBQS designation of the quasar is listed above each image pair. These are only the centers of the WFPC2 PC frames, sized to include all detectable emission from the host galaxies and any particularly close apparent companions.

Fig. 2.— Host galaxy absolute magnitude derived from (a) elliptical and (b) disk templates plotted against absolute magnitude of the quasar nuclear component. Filled circles are radio-loud quasars, and asterisks represent radio-quiet sources.

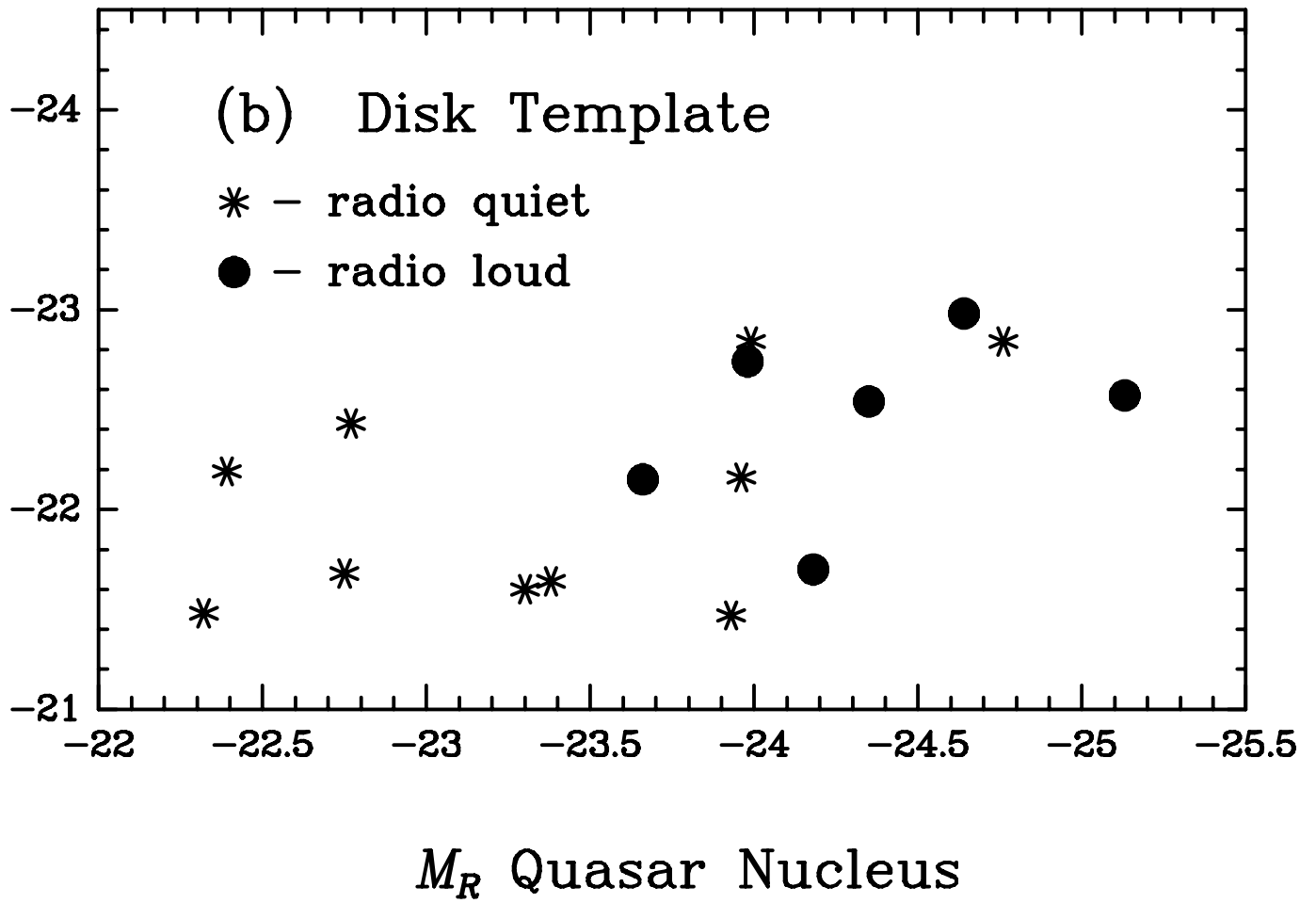
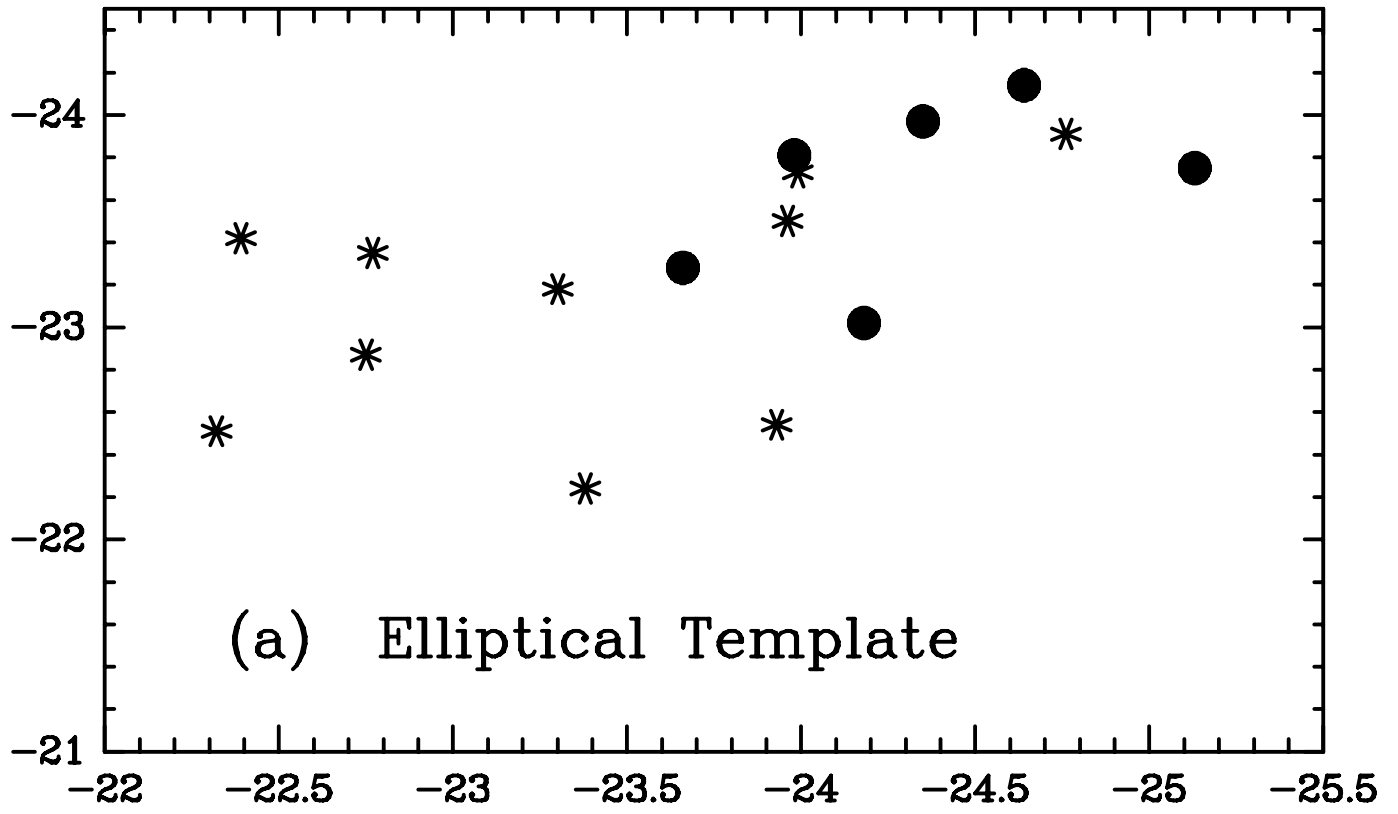
Table 1. Results of WFPC2 Analysis

Name (1)	z (2)	$\log L_{8.4}$ (W Hz $^{-1}$) (3)	R (quasar) (4)	M_R (quasar) (5)	R ($r^{1/4}$) (6)	M_R ($r^{1/4}$) (7)	R (disk) (8)	M_R (disk) (9)	axial ratio (10)
0020+0018	0.423	< 23.50	19.52	–22.39	19.33	–23.42	20.17	–22.19	0.7
0021–0301	0.422	< 23.50	19.15	–22.75	19.87	–22.87	20.67	–21.68	0.6
0100+0205	0.393	< 23.45	17.81	–23.93	19.97	–22.54	20.70	–21.47	0.3
1138+0003	0.500	25.60	17.94	–24.35	19.33	–23.97	20.26	–22.54	0.9
1149+0043	0.466	< 23.66	17.37	–24.76	19.17	–23.91	19.77	–22.84	0.6
1209+1259	0.418	< 23.52	19.56	–22.32	20.20	–22.51	20.85	–21.48	0.6
1218+1734	0.445	25.33	18.36	–23.66	19.63	–23.28	20.33	–22.15	0.6
1222+1010	0.398	< 23.46	18.46	–23.30	19.36	–23.18	20.59	–21.60	0.3
1222+1235	0.412	25.19	17.86	–23.98	18.85	–23.81	19.55	–22.74	0.6
1230–0015	0.470	25.77	17.51	–24.64	18.96	–24.14	19.65	–22.98	0.4
1240+1754	0.459	< 23.47	18.13	–23.96	19.50	–23.50	20.40	–22.16	0.3
1242–0123	0.491	< 23.47	18.26	–23.99	19.51	–23.73	19.91	–22.84	0.4
1243+1701	0.459	< 23.41	18.71	–23.38	20.84	–22.24	20.92	–21.64	0.1
2214–1903	0.397	< 23.48	18.98	–22.77	19.18	–23.35	19.75	–22.43	0.5
2348+0210	0.504	25.56	17.18	–25.13	19.57	–23.75	20.25	–22.57	0.4
2351–0036	0.460	26.40	17.92	–24.18	20.07	–23.02	20.87	–21.70	0.4

This figure "plate1pp.gif" is available in "gif" format from:

<http://arxiv.org/ps/astro-ph/9703085v1>

M_R Galaxy



This figure "plate2pp.gif" is available in "gif" format from:

<http://arxiv.org/ps/astro-ph/9703085v1>

This figure "plate3pp.gif" is available in "gif" format from:

<http://arxiv.org/ps/astro-ph/9703085v1>

This figure "plate4pp.gif" is available in "gif" format from:

<http://arxiv.org/ps/astro-ph/9703085v1>

This figure "plate5pp.gif" is available in "gif" format from:

<http://arxiv.org/ps/astro-ph/9703085v1>